Research Square

Preprints are preliminary reports that have not undergone peer review.
They should not be considered conclusive, used to inform clinical practice,
or referenced by the media as validated information.

Eosinophil Peroxidase–Associated PRKCB–CCL4/CCR5 Signaling in Chronic Rhinosinusitis with Nasal Polyps

Dan Wang
Qingdao University
Yu juan Yang
Qingdao University
Xianghuang Luo
Shaoguan Maternal and Child Health Hospital
Jing Guo
Qingdao University
Yingxue Li
Qingdao University
Yu Zhang
Qingdao University
Xicheng Song
drxchsong@163.com
Qingdao University

Research Article

Keywords: Chronic rhinosinusitis with nasal polyps, eosinophil peroxidase, proteomics, type 2 inflammation, chemokines

Posted Date: September 24th, 2026

DOI: https://doi.org/10.21203/rs.3.rs-10921512/v1

License: This work is licensed under a Creative Commons Attribution 4.0 International License.
Read Full License

Additional Declarations: No competing interests reported.

Version of Record: A version of this preprint was published at Inflammation on October 9th, 2026. See the published version at https://doi.org/10.1007/s10753-026-02623-2.

Abstract

Background

Eosinophil-derived effector molecules may contribute to persistent mucosal inflammation in chronic rhinosinusitis with nasal polyps (CRSwNP), but their effects on nasal epithelial responses remain incompletely understood. This study examined whether eosinophil peroxidase (EPX) contributes to CRSwNP-associated epithelial inflammation.

Methods

Data-independent acquisition–based quantitative proteomics was performed on nasal tissues from 69 patients with CRSwNP and 39 control subjects. Protein–protein interaction and weighted co-expression network analyses were used to identify candidate molecules, and EPX expression was validated in nasal tissues. The effects of EPX were examined through adeno-associated virus–mediated EPX knockdown in a murine CRSwNP model and recombinant EPX stimulation of human nasal epithelial cells, with or without PRKCB inhibition.

Results

Proteomic analysis identified 1,850 differentially expressed proteins, including 760 upregulated and 1,090 downregulated proteins. EPX was markedly upregulated in human CRSwNP tissues and murine nasal mucosa and was associated with eosinophilic inflammatory features. In mice, EPX knockdown attenuated nasal mucosal pathology and inflammatory cell infiltration and reduced IL-4, IL-5, IgE, PRKCB, CCL4, and CCR5 levels. In nasal epithelial cells, EPX increased PRKCB, CCL4, and CCR5 expression in a concentration-dependent manner, whereas PRKCB inhibition partially attenuated EPX-induced CCL4 and CCR5 upregulation.

Conclusions

EPX is associated with eosinophilic inflammation in CRSwNP and may contribute to nasal epithelial inflammatory responses involving the PRKCB–CCL4/CCR5 network. The mechanistic relevance of this network to CRSwNP warrants further investigation.

1. Introduction

Chronic rhinosinusitis with nasal polyps (CRSwNP) is characterized by heterogeneous inflammatory endotypes, with type 2 inflammation representing a prominent pattern in a substantial subset of patients [1]. This endotype is marked by eosinophilic infiltration and increased levels of type 2 inflammatory mediators, including IL-4, IL-5, IL-13, and IgE [2]. Despite advances in medical and surgical treatment,

patients with eosinophilic and type 2–dominant inflammation may experience persistent disease and recurrence, highlighting the need to better understand the mechanisms that sustain eosinophil-associated inflammation in CRSwNP [3, 4].

Eosinophils are key effector cells involved in type 2 inflammation in CRSwNP. Upon activation and degranulation, eosinophils release a variety of granule proteins and inflammatory mediators that contribute to epithelial barrier disruption, amplification of inflammatory responses, and recruitment of additional inflammatory cells [5–7]. However, the mechanisms by which eosinophil-derived effector molecules influence nasal epithelial cell responses and contribute to the maintenance of local inflammation remain incompletely understood.

Proteomic approaches enable systematic characterization of disease-associated molecular alterations at the protein level and provide a valuable strategy for identifying potential pathogenic molecules and therapeutic targets [8]. Recent studies have combined proteomic profiling with machine learning approaches to identify CRSwNP-associated biomarkers from nasal secretions and serum, providing new opportunities for inflammatory endotype classification and noninvasive diagnosis [9]. In the present study, we performed DIA-based quantitative proteomic analysis of nasal mucosal tissues from patients with CRSwNP and control subjects and identified eosinophil peroxidase (EPX) as a candidate molecule for further investigation.

We therefore integrated clinical tissue validation, AAV-mediated EPX knockdown in a mouse model, and in vitro EPX stimulation to investigate whether EPX contributes to local inflammatory responses in CRSwNP and to explore the underlying mechanisms.

Table 1
Baseline clinical characteristics of patients with CRSwNP and control subjects

Characteristics	CRSwNP group (n = 69)	Control group (n = 39)	P value
Sex (male/female)	51/18	27/12	0.602
Age group (< 50 years/≥50 years)	30/39	23/16	0.122
Smoking history, n (%)	24 (34.78%)	9 (23.08%)	0.205
Alcohol consumption, n (%)	18 (26.09%)	6 (15.38%)	0.199
Asthma, n (%)	14 (20.29%)	3 (7.69%)	0.084
Allergic rhinitis, n (%)	12 (17.39%)	0	0.004
Type 2 diabetes mellitus, n (%)	9 (13.04%)	1 (2.56%)	0.091
Hypertension, n (%)	14 (20.29%)	5 (12.82%)	0.327
Absolute eosinophil count (×10⁹/L), M (Q1, Q3)	0.28 (0.13, 0.41)	0.09 (0.06, 0.22)	< 0.001
Eosinophil percentage (%), M (Q1, Q3)	4.30 (2.40, 6.80)	1.50 (0.75, 3.35)	< 0.001
Absolute neutrophil count (×10⁹/L), M (Q1, Q3)	3.52 (2.81, 4.39)	2.96 (2.52, 5.00)	0.883
Neutrophil percentage (%), M (Q1, Q3)	53.60 (48.10, 58.80)	54.80 (47.95, 64.95)	0.314
Absolute monocyte count (×10⁹/L), M (Q1, Q3)	0.47 (0.34, 0.56)	0.45 (0.36, 0.54)	0.934
Monocyte percentage (%), M (Q1, Q3)	6.60 (5.60, 8.00)	7.20 (5.80, 8.15)	0.317
Absolute lymphocyte count (×10⁹/L), M (Q1, Q3)	2.09 (1.72, 2.52)	1.98 (1.75, 2.26)	0.352
Lymphocyte percentage (%), M (Q1, Q3)	33.80 (27.00, 39.60)	33.80 (25.30, 38.95)	0.855

Data are presented as n (%) for categorical variables and median (Q1, Q3) for continuous variables. Categorical variables were compared using Pearson's χ^2 test or Fisher's exact test when appropriate. Continuous variables were analyzed using the Mann–Whitney U test. A two-sided P value < 0.05 was considered statistically significant. Missing observations were excluded on a variable-by-variable basis.

2. Materials and Methods

2.1 Clinical samples and ethical approval

Nasal mucosal tissue samples were collected from patients who underwent surgery at the Department of Otorhinolaryngology, Head and Neck Surgery, Yantai Yuhuangding Hospital, between June 2020 and December 2021. A total of 69 patients with chronic rhinosinusitis with nasal polyps (CRSwNP) and 39 control subjects were included in this study. The collected tissues were subjected to DIA-based quantitative proteomic analysis, and the baseline clinical characteristics of the participants are summarized in Table 1. Selected tissue samples were further used for reverse transcription quantitative polymerase chain reaction (RT-qPCR) and Western blot validation.

Control tissues were obtained from the uncinate process or sinus mucosa of patients undergoing maxillary sinus cyst resection or optic nerve decompression surgery, whereas nasal polyp tissues were collected from patients with CRSwNP.

The inclusion criteria were as follows: (1) a confirmed diagnosis of CRSwNP according to the European Position Paper on Rhinosinusitis and Nasal Polyps (EPOS) 2020[10]; and (2) age ≥ 18 years. The exclusion criteria included: (1) concurrent malignancy or a history of malignancy; (2) use of intranasal or systemic corticosteroids within 1 month before surgery; (3) concomitant fungal rhinosinusitis, cystic fibrosis, or systemic immune disorders; and (4) aspirin-exacerbated respiratory disease (AERD).

This study was approved by the Ethics Committee of Yantai Yuhuangding Hospital (No. 2020 − 314), and written informed consent was obtained from all participants.

2.2 Proteomic analysis

2.2.1 Sample preparation

Nasal polyp tissues from patients with CRSwNP (n = 69) and control nasal mucosal tissues (n = 39), all stored at − 80°C, were used for protein extraction. Tissue samples were lysed using SDT buffer containing 4% sodium dodecyl sulfate (SDS), 100 mM dithiothreitol (DTT), and 150 mM Tris-HCl (pH 8.0). Following homogenization and centrifugation, protein-containing supernatants were collected, and protein concentrations were determined using the bicinchoninic acid (BCA) assay.

Equal amounts of protein from each sample were separated by SDS-PAGE for quality control and subsequently processed using the filter-aided sample preparation (FASP) method for protein reduction, alkylation, and enzymatic digestion. The digested peptides were desalted using C18 solid-phase extraction columns, lyophilized, and reconstituted in 0.1% formic acid solution.

For DIA mass spectrometry analysis, peptide samples were spiked with iRT peptides for retention time calibration. To generate a DDA-based spectral library, equal amounts of peptides from all samples were

pooled and fractionated using a high-pH reversed-phase peptide fractionation kit. The obtained fractions were subsequently analyzed by DDA mass spectrometry.

2.2.2 Mass spectrometry analysis

Ten peptide fractions obtained from high-pH reversed-phase fractionation were separated using an Evosep One nano-liquid chromatography system and analyzed by a timsTOF Pro mass spectrometer (Bruker Daltonics, Bremen, Germany) in data-dependent acquisition (DDA) mode to generate a spectral library for DIA analysis.

DDA acquisition was performed using the parallel accumulation–serial fragmentation (PASEF) mode. The mass range was set to m/z 100–1700, and the ion mobility range was set to 0.6–1.6 V·s/cm². Eight PASEF MS/MS scans were acquired in each cycle.

For DIA acquisition, peptide samples from individual tissues were separated using the same liquid chromatography system and analyzed in DIA mode. DIA was performed over an m/z range of 100–1700 with an additional ion mobility dimension. Variable isolation windows were determined based on the distribution of m/z values and ion mobility. During PASEF MS/MS acquisition, collision energy was dynamically adjusted as a function of ion mobility to achieve comprehensive proteome coverage.

2.2.3 Proteomic data analysis

Mass spectrometry data were analyzed using Spectronaut software (version 14.4.200727.47784, Biognosys). DDA data were searched against the UniProt human protein database (release 2021_03), and a project-specific spectral library was generated using iRT peptides for retention time calibration.

The database search parameters were as follows: trypsin was selected as the digestion enzyme, with a maximum of two missed cleavages allowed. Carbamidomethylation of cysteine residues was set as a fixed modification, whereas methionine oxidation and protein N-terminal acetylation were set as variable modifications. The false discovery rate (FDR) was controlled at 1% for protein identification.

DIA data were processed using the same version of Spectronaut software based on the established spectral library. Dynamic iRT calibration, MS2-level interference correction, and cross-run normalization were enabled during data processing. Proteins with a q value < 0.01 were retained for quantitative analysis, corresponding to an FDR of < 1%.

2.3 Bioinformatics analysis

2.3.1 Identification of differentially expressed proteins

Differential expression analysis was performed using the normalized protein abundance matrix. Between-group differences were assessed using an unpaired t test. Differentially expressed proteins (DEPs) were defined by a mean CRSwNP-to-control fold change (FC) > 1.5 or < 0.67 and P value < 0.05.

Proteins meeting these criteria were classified as upregulated or downregulated and included in subsequent bioinformatics analyses.

2.3.2 Functional enrichment analysis

Gene Ontology (GO) annotation and enrichment analyses of differentially expressed proteins were performed using Blast2GO software. The GO analysis included three major categories: biological process (BP), molecular function (MF), and cellular component (CC). In addition, differentially expressed proteins were mapped to the Kyoto Encyclopedia of Genes and Genomes (KEGG) database for pathway enrichment analysis.

Enrichment significance was assessed using Fisher's exact test, with all quantified proteins as the background set. P values were adjusted using the Benjamini–Hochberg method, and pathways or functional categories with a false discovery rate (FDR) < 0.05 were considered significantly enriched.

2.3.3 Correlation and protein–protein interaction network analyses

Pearson's correlation coefficients between EPX and all quantified proteins were calculated using the normalized protein abundance matrix. Proteins correlated with EPX expression ($|r| > 0.6$) were submitted to the STRING database (https://string-db.org/; *Homo sapiens*) to construct and visualize a protein–protein interaction network.

2.3.4 Weighted gene co-expression network analysis

Weighted gene co-expression network analysis (WGCNA) was performed using the WGCNA package (version 1.69) in R software. A co-expression network was constructed based on the $\log_2$-transformed protein abundance matrix. The optimal soft-thresholding power was determined to establish a scale-free network topology, and protein modules were identified using the dynamic tree cut algorithm.

Module eigengenes were subsequently correlated with clinical characteristics, including eosinophil counts, neutrophil counts, and computed tomography (CT) scores, to identify key protein modules and candidate proteins associated with CRSwNP-related disease phenotypes.

2.4 Cell culture and treatment

Human nasal epithelial cells (HNEpCs; BNCC356247, BeNa Culture Collection, Beijing, China) were cultured in minimum essential medium (MEM) supplemented with 10% fetal bovine serum (FBS) and 1% penicillin–streptomycin under a humidified atmosphere containing 5% CO2 at 37°C.

To evaluate the effects of EPX on inflammatory molecule expression, HNEpCs were stimulated with recombinant EPX (Cloud-Clone Corp., Wuhan, China) at 0, 100, 200, 400, or 800 ng/mL for 24 h. To assess the involvement of PRKCB in EPX-induced responses, HNEpCs were pretreated with PKCβ inhibitor 1 (20 μM; cat. no. S87666; Shanghai Yuanye Bio-Technology Co., Ltd., Shanghai, China) and then

incubated with EPX (800 ng/mL) for 24 h. The relevant inflammatory molecules were subsequently analyzed.

2.5 CRSwNP mouse model establishment and EPX knockdown intervention

Male C57BL/6 mice aged 6–8 weeks (n = 30) were purchased from Jinan Pengyue Laboratory Animal Breeding Co., Ltd. All animal experiments were approved by the Ethics Committee of Yantai Yuhuangding Hospital (No. K2026-353) and performed in accordance with the institutional guidelines for animal care and use.

After one week of acclimatization, the mice were randomly assigned to three groups (n = 10 per group): the control group (intranasal PBS administration), the CRSwNP + AAV-NC group, and the CRSwNP + AAV-shEPX group. For brevity, the CRSwNP + AAV-NC and CRSwNP + AAV-shEPX groups are hereafter referred to as the CRSwNP and CRSwNP/shEPX groups, respectively. A murine model of CRSwNP was established according to a previously reported protocol (Kim et al.[11]). Briefly, Aspergillus protease (AP; 2 U) and ovalbumin (OVA; 75 μg) were dissolved in PBS and administered intranasally (20 μL per mouse) three times weekly for 12 consecutive weeks. Control mice received an equivalent volume of PBS according to the same schedule.

Beginning in week 10 of model induction, mice in the CRSwNP/shEPX group received intranasal administration of EPX-targeting AAV-shEPX (2×10^9 TU/mL, 20 μL per mouse; Genechem, Shanghai, China) three times weekly for 2 weeks. Mice in the CRSwNP group received the corresponding AAV-NC using the same procedure.

Twenty-four hours after the final administration, the mice were euthanized, and serum and nasal mucosal tissues were collected. Nasal tissues were either stored at − 80°C for molecular analyses or processed for histological examination. Three mice from each group were randomly selected for RT-qPCR and Western blotting, whereas the remaining samples were used for histological evaluation, ELISA, or stored for further analyses. The exact biological sample size used for each assay is indicated in the corresponding figure legend.

2.6 Hematoxylin and eosin (H&E) and periodic acid–Schiff (PAS) staining

For histological examination, nasal tissues were fixed in 4% paraformaldehyde, decalcified, and embedded in paraffin. Paraffin sections (4 μm thick) were prepared and subjected to H&E and PAS staining. Sections were stained with hematoxylin and eosin (SparkJade, China) to evaluate nasal mucosal morphology and inflammatory changes. PAS staining was performed using a commercial PAS staining kit (Solarbio, China) to assess goblet cell hyperplasia and mucus production. Histological changes were examined under a light microscope, and representative images were captured.

2.7 Reverse transcription quantitative polymerase chain reaction (RT-qPCR)

Total RNA was extracted from nasal tissues and cultured cells using TRIzol reagent. Complementary DNA (cDNA) was synthesized using a reverse transcription kit according to the manufacturer's instructions. RT-qPCR was performed using cDNA as the template to determine the expression levels of target genes.

Relative gene expression levels were calculated using the $2^{-\Delta\Delta Ct}$ method, with GAPDH used as the endogenous control. The primer sequences used in this study are listed in Supplementary Table S1.

2.8 Western blotting

Total protein was extracted from mouse nasal mucosal tissues and cultured cells using RIPA lysis buffer supplemented with PMSF. After lysis and centrifugation, the supernatants were collected, and protein concentrations were determined using the BCA assay. Equal amounts of protein were separated by SDS-PAGE and transferred onto PVDF membranes. The membranes were blocked with 5% nonfat milk and incubated at 4°C overnight with primary antibodies against EPX (Proteintech, Wuhan, China; 1:1,000), PRKCB and CCR5 (ImmunoWay; 1:1,000), GAPDH (Abmart, Shanghai, China; 1:10,000), and β-tubulin (ImmunoWay; 1:10,000).

After incubation with HRP-conjugated secondary antibodies (Affinity Biosciences; 1:5,000), protein bands were visualized using an ECL detection system. The images were captured, and band intensities were quantified using ImageJ software. The relative expression levels of target proteins were normalized to the corresponding loading control proteins.

2.9 ELISA

ELISA kits (Genemed, China) were used to measure the levels of IL-4, IL-5, IgE, and CCL4 in mouse serum, nasal mucosal tissue homogenates, and cell culture supernatants. All procedures were performed according to the manufacturer's instructions. After incubation, washing, and color development, absorbance was measured at 450 nm, and the concentrations of target molecules were calculated based on the standard curves.

2.10 Statistical analysis

Statistical analyses were performed using GraphPad Prism version 9.0. Continuous data are presented as the mean ± standard deviation or median (interquartile range), according to their distribution, and categorical data as n (%). Two-group comparisons were performed using an unpaired two-tailed Student's *t* test or Mann–Whitney *U* test. Multiple-group comparisons were performed using one-way ANOVA followed by Tukey's test or the Kruskal–Wallis test followed by Dunn's test. Correlations were assessed using Pearson's correlation analysis. Categorical variables were compared using Pearson's χ^2 test or Fisher's exact test. All tests were two-sided, and $P < 0.05$ was considered statistically significant.

3. Results

3.1 Proteomic data quality control, identification of differentially expressed proteins, and functional analysis

To evaluate the reliability of the proteomic data, quality control analyses were performed based on sample correlation, quantitative stability, and overall data distribution. The sample correlation heatmap showed strong agreement among quality control (QC) samples, with most correlation coefficients exceeding 0.93, indicating high reproducibility of protein quantification (Fig. 1A). The coefficient of variation (CV) analysis of protein abundance in QC samples showed low overall variability, with a median CV of approximately 11%, and the CV values of most quantified proteins were below 20%, suggesting high repeatability and quantitative stability of the mass spectrometry analysis (Fig. 1B).

Principal component analysis (PCA) revealed a clear separation trend between CRSwNP and control samples, while QC samples clustered tightly, supporting good technical reproducibility (Fig. 1C). In total, 132,310 peptides were identified and 8,954 proteins were quantified. Using the criteria of FC > 1.5 or < 0.67 and P value < 0.05, 1,850 DEPs were identified, including 760 upregulated and 1,090 downregulated proteins. Their distribution is shown in the volcano plot (Fig. 1D).

Functional annotation and enrichment analysis showed that the differentially expressed proteins were mainly involved in cellular processes, biological regulation, metabolic processes, localization, response to stimulus, and immune system processes. In terms of molecular function, the proteins were mainly associated with binding, catalytic activity, transporter activity, and molecular function regulator categories. With regard to cellular component, they were mainly localized to cellular anatomical entities, organelles, membranes, extracellular regions, and protein-containing complexes (Fig. 1E). KEGG pathway analysis showed that the differentially expressed proteins were mainly enriched in complement and coagulation cascades, infection-related pathways, the PI3K–Akt signaling pathway, the Rap1 signaling pathway, focal adhesion, and regulation of the actin cytoskeleton (Fig. 1F). These results suggest that dysregulated protein expression in CRSwNP tissues involves multiple biological processes, including immune and inflammatory responses, cell adhesion and migration, and signal transduction. Among the differentially expressed proteins, EPX was markedly upregulated in CRSwNP tissues, with a mean CRSwNP-to-control abundance ratio of 82.19 ($P = 5.29 \times 10^{-9}$). Given the close association of EPX with eosinophil-related inflammatory features, subsequent functional validation focused on EPX (Fig. 1G).

(A) Heatmap showing the correlation of protein expression profiles among samples. (B) Distribution of protein quantification CV values in QC samples. (C) PCA plot showing the separation of CRSwNP and control samples with tight clustering of QC samples. (D) Volcano plot showing differentially expressed proteins between CRSwNP and control groups; EPX was significantly upregulated in CRSwNP tissues. (E) GO enrichment analysis of differentially expressed proteins. (F) KEGG pathway enrichment analysis showing the involvement of immune-related and signaling pathways. (G) Relative abundance of EPX identified by proteomic analysis in CRSwNP and control groups. ****P<0.0001

3.2 EPX is upregulated in nasal mucosal tissues of patients with CRSwNP

EPX expression was evaluated in nasal mucosal tissues from control subjects and nasal polyp tissues from patients with CRSwNP. RT-qPCR and Western blotting analyses showed that *EPX* mRNA and EPX protein levels were significantly increased in CRSwNP tissues compared with control tissues ($P < 0.05$, Fig. 2A). These results demonstrate that EPX is upregulated in CRSwNP tissues and suggest its potential involvement in CRSwNP-associated inflammatory processes.

3.3 EPX knockdown alleviates nasal mucosal pathological changes and inflammatory responses in a CRSwNP mouse model

To further investigate the potential role of EPX in CRSwNP, a murine CRSwNP model was established, and EPX expression was silenced using AAV-shEPX (Fig. 2B). H&E and PAS staining revealed that, compared with control mice, CRSwNP model mice exhibited marked nasal mucosal thickening, epithelial structural damage, increased inflammatory cell infiltration, and enhanced PAS-positive mucus production, indicating the establishment of CRSwNP-like pathological changes. Following AAV-shEPX intervention, mucosal thickening was reduced, inflammatory cell infiltration was attenuated, and PAS-positive areas were significantly decreased ($P < 0.05$, Fig. 2C).

Further analysis showed that *Epx* mRNA and EPX protein levels were significantly increased in the nasal mucosal tissues of CRSwNP model mice compared with control mice ($P < 0.05$, Fig. 2D). Treatment with AAV-shEPX markedly reduced both *Epx* mRNA and EPX protein levels ($P < 0.05$), confirming the efficiency of EPX knockdown. In addition, compared with the CRSwNP model group, mice treated with AAV-shEPX exhibited significantly decreased serum IgE levels and reduced IL-4 and IL-5 levels in nasal mucosal tissues ($P < 0.05$, Fig. 2E).

Collectively, these findings demonstrate that EPX knockdown attenuates nasal mucosal pathological alterations and suppresses type 2 inflammatory responses in the CRSwNP mouse model, suggesting that EPX may contribute to CRSwNP-associated inflammation.

(A) Human *EPX* mRNA and EPX protein levels in nasal polyp tissues from patients with CRSwNP were detected by RT-qPCR and Western blotting. **(B)** Schematic diagram showing the establishment of the CRSwNP mouse model and AAV-shEPX intervention protocol. **(C)** Representative images of H&E staining (upper panels) and PAS staining (lower panels) of nasal mucosal tissues from different groups, with quantification of eosinophil infiltration and PAS-positive goblet cells. Scale bars: 800 μm and 50 μm. **(D)** Mouse *Epx* mRNA and EPX protein levels in nasal mucosal tissues were determined by RT-qPCR and Western blotting. **(E)** IL-4 and IL-5 levels in nasal mucosal tissues and serum IgE levels were measured by ELISA. *P<0.05, **P<0.01, ***P<0.001, ****P<0.0001

3.4 Association of EPX with PRKCB and identification of disease-related protein modules in CRSwNP

To investigate EPX-associated protein networks, proteins significantly correlated with EPX expression (|r| > 0.6) were selected to construct a protein–protein interaction (PPI) network (Fig. 3A). Correlation analysis revealed a significant positive correlation between EPX and PRKCB protein abundance ($r = 0.699$, $P = 3.90 \times 10^{-22}$).

WGCNA was further performed based on the proteomic expression matrix to identify disease-associated protein modules. Among the identified co-expression modules, the brown module showed significant correlations with clinical and inflammatory characteristics. The module eigengene of the brown module (MEbrown), representing the overall expression pattern of this module, was used for module–trait correlation analysis. Both EPX and PRKCB were assigned to the brown module.

Module–trait correlation analysis demonstrated that MEbrown was positively correlated with bilateral sinus CT scores, total CT scores, eosinophil-related inflammatory parameters, and endoscopic scores ($r = 0.52–0.69$). In addition, MEbrown showed positive correlations with peripheral blood eosinophil counts and related inflammatory phenotypes ($r = 0.35–0.65$), as well as neutrophil-related parameters ($r = 0.44–0.68$) (Fig. 3B).

Within the brown module, EPX and PRKCB had high module membership (MM) values (0.8012 and 0.7503, respectively). PS–MM analysis showed significant positive correlations between MM and protein significance (PS) for eosinophil-related traits. The correlations between MM and PS for peripheral blood eosinophil counts and proportions were 0.54 and 0.52, respectively (Fig. 3C–D). For inflammatory phenotypes defined by eosinophil counts and proportions, the corresponding correlations were 0.77 and 0.72. EPX had higher PS values than PRKCB for eosinophil-related traits, while both proteins showed high module connectivity.

Collectively, the PPI analysis linked EPX with PRKCB, while WGCNA assigned both proteins to the brown module, which was associated with CRSwNP severity and inflammatory phenotypes.

3.5 Effects of EPX knockdown on PRKCB/CCL4/CCR5 expression in a CRSwNP mouse model

Based on the PPI network and WGCNA analyses, PRKCB was identified as a candidate protein associated with EPX expression. Given the involvement of PRKCB-related inflammatory signaling and the role of the CCL4/CCR5 chemokine axis in immune cell recruitment, we further evaluated changes in the expression of PRKCB and CCL4/CCR5-related molecules following AAV-shEPX intervention in the CRSwNP mouse model.

Compared with control mice, CRSwNP model mice exhibited significantly increased mRNA levels of *Prkcb*, *Ccl4*, and *Ccr5* in nasal mucosal tissues. AAV-shEPX intervention significantly reduced the mRNA levels of these genes compared with the CRSwNP model group ($P < 0.05$, Fig. 4A–C).

Consistent with the transcriptional changes, Western blotting and ELISA analyses demonstrated that PRKCB and CCR5 protein expression levels, as well as CCL4 protein levels, were significantly elevated in nasal mucosal tissues of CRSwNP model mice. Following EPX knockdown, the expression levels of PRKCB, CCR5, and CCL4 were markedly decreased ($P < 0.05$, Fig. 4D–G).

Together, these findings show that PRKCB, CCL4, and CCR5 levels are increased in the CRSwNP mouse model and reduced after EPX knockdown, supporting an association between EPX and the PRKCB–CCL4/CCR5 inflammatory network.

3.6 PRKCB inhibition attenuates EPX-induced expression of CCL4/CCR5-related molecules in HNEpCs

To further investigate the involvement of PRKCB in EPX-associated regulation of the CCL4/CCR5 inflammatory axis, in vitro experiments were performed using human nasal epithelial cells (HNEpCs). HNEpCs were stimulated with different concentrations of EPX, and changes in the expression of PRKCB, CCL4, and CCR5 were evaluated. RT-qPCR showed that EPX stimulation increased *PRKCB*, *CCL4*, and *CCR5* mRNA levels in a concentration-dependent manner (Fig. 5A–C).

To determine whether PRKCB contributes to EPX-induced inflammatory responses, HNEpCs were pretreated with a PRKCB inhibitor before EPX stimulation. Compared with the control group, EPX stimulation significantly increased the mRNA levels of *PRKCB*, *CCL4*, and *CCR5*, whereas PRKCB inhibition markedly reduced the mRNA levels of these genes compared with EPX stimulation alone ($P < 0.05$, Fig. 5D–F).

Consistent with the transcriptional changes, Western blotting analysis demonstrated that EPX stimulation increased PRKCB and CCR5 protein expression in HNEpCs, while PRKCB inhibition significantly attenuated these changes ($P < 0.05$, Fig. 5G). Furthermore, ELISA analysis showed that EPX stimulation increased CCL4 secretion in cell culture supernatants, whereas PRKCB inhibition significantly reduced CCL4 levels ($P < 0.05$, Fig. 5H).

4. Discussion

Eosinophil-derived effector molecules can regulate nasal epithelial responses and local inflammatory networks, potentially sustaining inflammation in CRSwNP [12]. In this study, we integrated DIA-based quantitative proteomics, co-expression network analysis, clinical tissue validation, a mouse model, and in vitro experiments to examine the role of EPX in CRSwNP-associated type 2 inflammation. EPX was upregulated and associated with eosinophilic inflammatory phenotypes. These findings are consistent with previous studies showing that EPX is associated with tissue eosinophilia and may serve as a

biomarker for eosinophilic CRS [13]. In the mouse model, EPX knockdown ameliorated nasal mucosal pathology and reduced PRKCB, CCL4, and CCR5 expression. In nasal epithelial cells, EPX stimulation increased their expression, whereas PRKCB inhibition partially attenuated EPX-induced CCL4/CCR5 responses. Together, these findings implicate EPX in epithelial inflammatory and chemokine responses associated with the PRKCB–CCL4/CCR5 network.

EPX is a heme peroxidase released during eosinophil activation and degranulation. It generates reactive oxidants from hydrogen peroxide and halide substrates, contributing to host defense under physiological conditions [14, 15]. However, persistent eosinophil activation and excessive EPX release in chronic inflammatory settings may promote oxidative stress, tissue injury, and epithelial barrier dysfunction. Previous studies have associated EPX levels with the severity of local type 2 inflammation, IL-5 expression, and multiple inflammatory mediators in CRSwNP [13, 16, 17]. Together with previous evidence, our findings suggest that, beyond reflecting eosinophil activation, EPX may influence the inflammatory microenvironment by altering nasal epithelial responses.

Our proteomic and enrichment analyses showed that DEPs in CRSwNP were associated primarily with immune regulation, complement activation, inflammatory cell recruitment, and signal transduction. Growing evidence indicates that nasal epithelial cells are not merely passive targets of inflammatory injury but also actively regulate local immune responses. Previous studies have demonstrated prominent epithelial remodeling in CRSwNP, with IL-13-associated epithelial changes correlating with disease severity [18, 19]. Abnormal basal cells in eosinophilic CRSwNP can also amplify type 2 inflammation through the secretion of TSLP [19, 20]. Thus, interactions between eosinophil-derived effector molecules and nasal epithelial cells may help sustain local inflammation.

PRKCB emerged as a candidate component of the EPX-associated inflammatory network in our analysis. The biological plausibility of this association is supported by previous evidence demonstrating PKCβ expression and activity in human eosinophils [21]. PPI analysis linked EPX to several inflammation-related proteins, including PRKCB, and WGCNA assigned both EPX and PRKCB to a co-expression module associated with eosinophilic phenotypes and disease severity in CRSwNP.

PRKCB, a member of the protein kinase C family, has been implicated in immune cell activation, NF-κB-related signaling, and inflammatory mediator expression. Previous studies have shown that PKCβ can regulate IKKα phosphorylation and NF-κB activation in B cells [22]. Together with our findings, these observations suggest that PRKCB may link EPX-associated molecular changes to downstream chemokine responses.

In the CRSwNP mouse model, PRKCB, CCL4, and CCR5 levels were increased, whereas EPX knockdown reduced their expression. Similarly, EPX stimulation upregulated PRKCB, CCL4, and CCR5 in nasal epithelial cells, while PRKCB inhibition partially attenuated these changes.

CCL4, an important CCR5 ligand, promotes the recruitment and activation of immune cells and has been implicated in chronic airway inflammation and local inflammatory responses in CRSwNP [7, 23, 24].

Previous studies have also suggested that CCR5 activation may involve PKC-dependent phosphorylation and receptor-associated signaling [25–27]. Although the CCL4/CCR5 axis has been implicated in eosinophil-associated airway inflammation and CRSwNP pathogenesis, its relationship to EPX remains unclear. The coordinated effects of EPX knockdown, exogenous EPX, and PRKCB inhibition observed here suggest that EPX may regulate CCL4/CCR5-mediated chemokine responses through PRKCB-associated signaling.

Current biologic therapies for CRSwNP mainly target canonical type 2 pathways, including IL-4/IL-13, IL-5, and IgE signaling [28, 29]. EPX may provide a molecular link between eosinophil activation and nasal epithelial inflammation, and the associated PRKCB–CCL4/CCR5 network warrants further mechanistic and translational investigation.

Several limitations should be acknowledged. First, we used AAV-mediated EPX knockdown rather than a genetic knockout model to examine EPX function in CRSwNP inflammation. Conditional EPX knockout models are therefore needed to clarify its cellular source and causal role in pathogenesis. Second, we focused on the association between EPX and the PRKCB–CCL4/CCR5 network. Although the findings suggest that EPX may regulate CCL4/CCR5 responses through PRKCB-associated signaling, whether EPX directly regulates PRKCB activation and how this network affects inflammatory-cell recruitment and the local immune microenvironment remain to be determined.

5. Conclusion

In conclusion, EPX was upregulated in CRSwNP tissues and associated with eosinophilic inflammatory phenotypes. EPX knockdown ameliorated nasal mucosal inflammation in a CRSwNP mouse model and reduced PRKCB, CCL4, and CCR5 expression. In nasal epithelial cells, PRKCB inhibition partially attenuated EPX-induced CCL4 and CCR5 upregulation. These findings implicate EPX in CRSwNP-associated inflammation and support further investigation of PRKCB-related CCL4/CCR5 signaling as a potential mechanism.

Declarations

Conflict of Interest

The authors declare no conflicts of interest.

Funding

This work was supported by the National Natural Science Foundation of China (Nos. 82271146, 82271147, 82571287, and 82501379) and the Major Scientific and Technological Innovation Project of Shandong Province (No. 2022CXGC020506).

Author Contribution

Dan Wang drafted the manuscript. Yujuan Yang and Xianghuang Luo contributed to manuscript preparation and revision. Jing Guo and Yingxue Li prepared the figures. Yu Zhang and Xicheng Song critically revised and reviewed the manuscript. All authors reviewed and approved the final manuscript.

Acknowledgement

The authors thank all participants for their contribution to this study.

Data Availability

The datasets generated and/or analysed during the current study are available from the corresponding author on reasonable request.

References

1. Cardell, L.O., et al., *Endotypes of chronic rhinosinusitis: Impact on management.* J Allergy Clin Immunol, 2020. **145**(3): p. 752-756.http://doi.org/10.1016/j.jaci.2020.01.019.
2. Bachert, C., et al., *The interleukin-4/interleukin-13 pathway in type 2 inflammation in chronic rhinosinusitis with nasal polyps.* Front Immunol, 2024. **15**: p. 1356298.http://doi.org/10.3389/fimmu.2024.1356298.
3. Martin-Jimenez, D., et al., *Endoscopic Extended Sinus Surgery for Patients with Severe Chronic Rhinosinusitis with Nasal Polyps, the Choice of Mucoplasty: A Systematic Review.* Curr Allergy Asthma Rep, 2023. **23**(12): p. 733-746.http://doi.org/10.1007/s11882-023-01113-x.
4. Borish, L., et al., *Evaluating enrollment and outcome criteria in trials of biologics for chronic rhinosinusitis with nasal polyps.* Ann Allergy Asthma Immunol, 2022. **129**(2): p. 160-168.http://doi.org/10.1016/j.anai.2022.04.004.
5. Bochner, B.S. and W.W. Stevens, *Biology and Function of Eosinophils in Chronic Rhinosinusitis With or Without Nasal Polyps.* Allergy Asthma Immunol Res, 2021. **13**(1): p. 8-22.http://doi.org/10.4168/aair.2021.13.1.8.
6. Shin, S.H., et al., *Immunopathologic Role of Eosinophils in Eosinophilic Chronic Rhinosinusitis.* Int J Mol Sci, 2022. **23**(21).http://doi.org/10.3390/ijms232113313.
7. Chu, H.H., et al., *CCL4 Regulates Eosinophil Activation in Eosinophilic Airway Inflammation.* Int J Mol Sci, 2022. **23**(24).http://doi.org/10.3390/ijms232416149.
8. Aebersold, R. and M. Mann, *Mass-spectrometric exploration of proteome structure and function.* Nature, 2016. **537**(7620): p. 347-55.http://doi.org/10.1038/nature19949.

9. Hou, Y., et al., *Proteomic profiling of nasal fluids and serum for type 2 nasal polyps diagnosis.* Ann Allergy Asthma Immunol, 2025. **135**(2): p. 186-196.e30.http://doi.org/10.1016/j.anai.2025.04.007.
10. Fokkens, W.J., et al., *European Position Paper on Rhinosinusitis and Nasal Polyps 2020.* Rhinology, 2020. **58**(Suppl S29): p. 1-464.http://doi.org/10.4193/Rhin20.600.
11. Kim, H.C., et al., *Development of a mouse model of eosinophilic chronic rhinosinusitis with nasal polyp by nasal instillation of an Aspergillus protease and ovalbumin.* Eur Arch Otorhinolaryngol, 2017. **274**(11): p. 3899-3906.http://doi.org/10.1007/s00405-017-4717-2.
12. Tsuda, T., et al., *Eosinophil-derived neurotoxin enhances airway remodeling in eosinophilic chronic rhinosinusitis and correlates with disease severity.* Int Immunol, 2019. **31**(1): p. 33-40.http://doi.org/10.1093/intimm/dxy061.
13. Idler, B.M., et al., *Eosinophil Peroxidase: A Biomarker for Eosinophilic Chronic Rhinosinusitis Agnostic of Polyp Status.* Laryngoscope, 2024. **134**(1): p. 69-78.http://doi.org/10.1002/lary.30787.
14. Khan, A.A., M.A. Alsahli, and A.H. Rahmani, *Myeloperoxidase as an Active Disease Biomarker: Recent Biochemical and Pathological Perspectives.* Med Sci (Basel), 2018. **6**(2).http://doi.org/10.3390/medsci6020033.
15. van Dalen, C.J., C.C. Winterbourn, and A.J. Kettle, *Mechanism of nitrite oxidation by eosinophil peroxidase: implications for oxidant production and nitration by eosinophils.* Biochem J, 2006. **394**(Pt 3): p. 707-13.http://doi.org/10.1042/bj20051470.
16. Callander, J.K., et al., *In office sampling of eosinophil peroxidase to diagnose eosinophilic chronic rhinosinusitis.* Int Forum Allergy Rhinol, 2025. **15**(1): p. 36-44.http://doi.org/10.1002/alr.23448.
17. Motojima, S., et al., *Eosinophil peroxidase stimulates the release of granulocyte-macrophage colony-stimulating factor from bronchial epithelial cells.* J Allergy Clin Immunol, 1996. **98**(6 Pt 2): p. S216-23.http://doi.org/10.1016/s0091-6749(96)70069-6.
18. Wynne, M., et al., *Contribution of Epithelial Cell Dysfunction to the Pathogenesis of Chronic Rhinosinusitis with Nasal Polyps.* Am J Rhinol Allergy, 2019. **33**(6): p. 782-790.http://doi.org/10.1177/1945892419868588.
19. Kotas, M.E., et al., *IL-13-associated epithelial remodeling correlates with clinical severity in nasal polyposis.* J Allergy Clin Immunol, 2023. **151**(5): p. 1277-1285.http://doi.org/10.1016/j.jaci.2022.12.826.
20. Kawakita, K., et al., *Role of basal cells in nasal polyp epithelium in the pathophysiology of eosinophilic chronic rhinosinusitis (eCRS).* Allergol Int, 2024. **73**(4): p. 563-572.http://doi.org/10.1016/j.alit.2024.04.001.
21. Bates, M.E., et al., *Increased protein kinase C activity in low density eosinophils.* J Immunol, 1993. **150**(10): p. 4486-93
22. Saijo, K., et al., *Protein kinase C beta controls nuclear factor kappaB activation in B cells through selective regulation of the IkappaB kinase alpha.* J Exp Med, 2002. **195**(12): p. 1647-52.http://doi.org/10.1084/jem.20020408.

23. Kobayashi, Y., et al., *Critical role of CCL4 in eosinophil recruitment into the airway.* Clin Exp Allergy, 2019. **49**(6): p. 853-860.http://doi.org/10.1111/cea.13382.
24. Kobayashi, Y., et al., *CCL4 Functions as a Biomarker of Type 2 Airway Inflammation.* Biomedicines, 2022. **10**(8).http://doi.org/10.3390/biomedicines10081779.
25. Silva, T., et al., *The Chemokine CCL5 Inhibits the Replication of Influenza A Virus Through SAMHD1 Modulation.* Front Cell Infect Microbiol, 2021. **11**: p. 549020.http://doi.org/10.3389/fcimb.2021.549020.
26. Alfano, M., et al., *The B-oligomer of pertussis toxin deactivates CC chemokine receptor 5 and blocks entry of M-tropic HIV-1 strains.* J Exp Med, 1999. **190**(5): p. 597-605.http://doi.org/10.1084/jem.190.5.597.
27. Pollok-Kopp, B., et al., *Analysis of ligand-stimulated CC chemokine receptor 5 (CCR5) phosphorylation in intact cells using phosphosite-specific antibodies.* J Biol Chem, 2003. **278**(4): p. 2190-8.http://doi.org/10.1074/jbc.M209844200.
28. Wautlet, A., et al., *The Management of Chronic Rhinosinusitis With Nasal Polyps (CRSwNP) With Biologics.* J Allergy Clin Immunol Pract, 2023. **11**(9): p. 2642-2651.http://doi.org/10.1016/j.jaip.2023.04.054.
29. Papacharalampous, G.X., et al., *Chronic rhinosinusitis with nasal polyps (CRSwNP) treated with omalizumab, dupilumab, or mepolizumab: A systematic review of the current knowledge towards an attempt to compare agents' efficacy.* Int Forum Allergy Rhinol, 2024. **14**(1): p. 96-109.http://doi.org/10.1002/alr.23234.

Figures

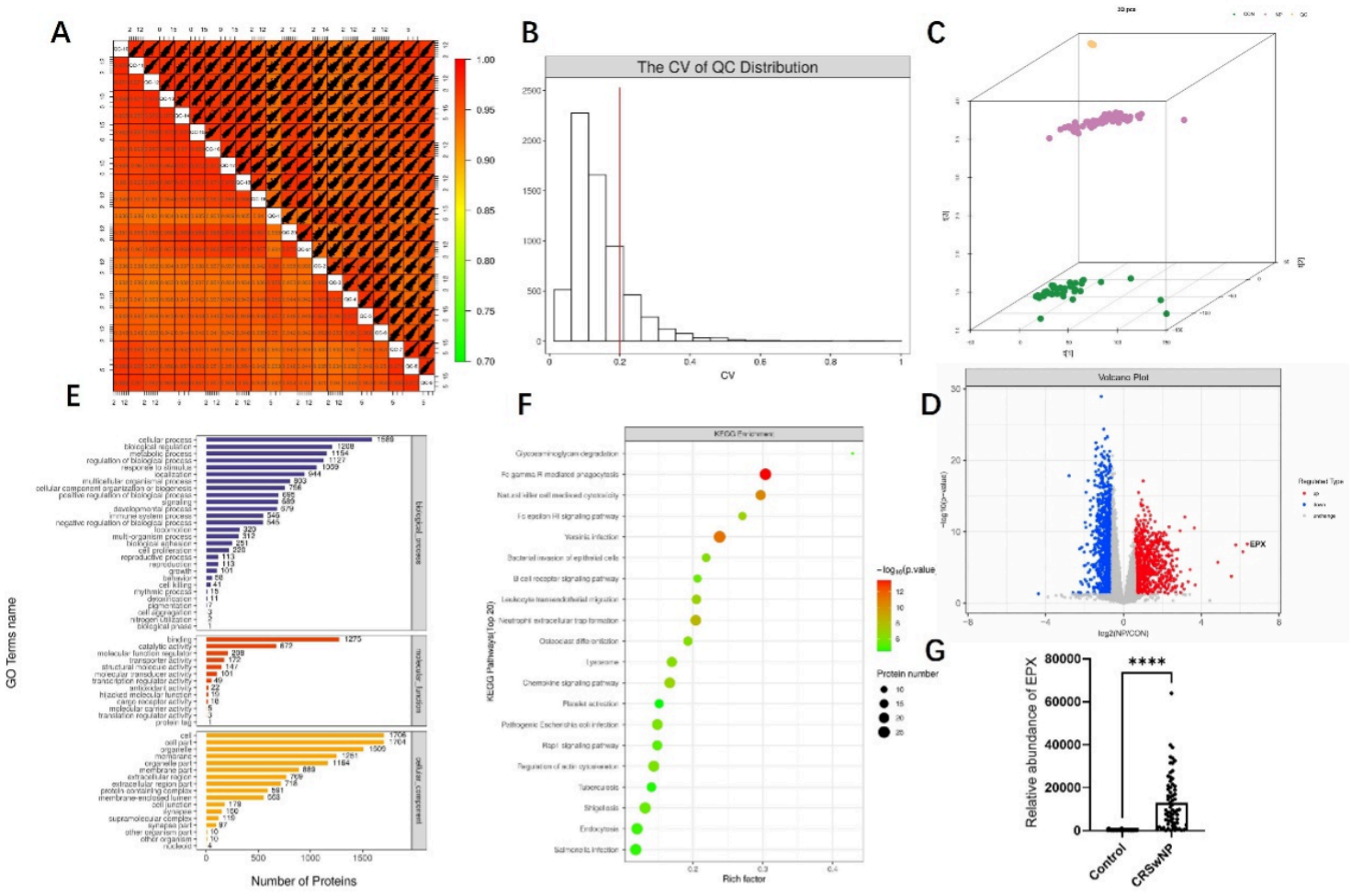


Figure 1

Identification, quality control, and functional analysis of differentially expressed proteins in CRSwNP. (A) Heatmap showing the correlation of protein expression profiles among samples. (B) Distribution of protein quantification CV values in QC samples. (C) PCA plot showing the separation of CRSwNP and control samples with tight clustering of QC samples. (D) Volcano plot showing differentially expressed proteins between CRSwNP and control groups; EPX was significantly upregulated in CRSwNP tissues. (E) GO enrichment analysis of differentially expressed proteins. (F) KEGG pathway enrichment analysis showing the involvement of immune-related and signaling pathways. (G) Relative abundance of EPX identified by proteomic analysis in CRSwNP and control groups. ****P□0.0001

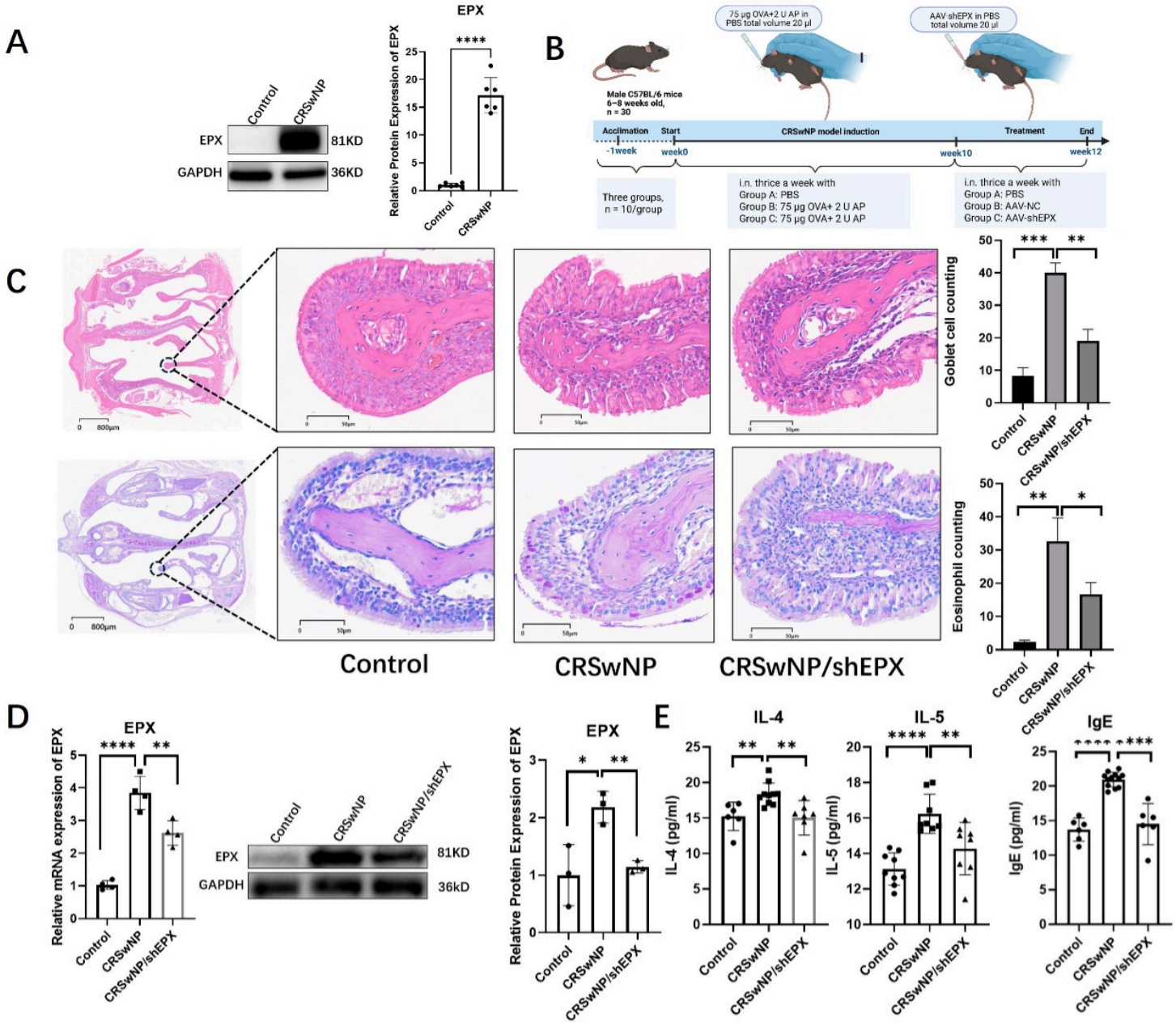


Figure 2

EPX is upregulated in CRSwNP tissues and the mouse model, and EPX knockdown attenuates nasal mucosal pathology and type 2 inflammation.

(A) Human *EPX* mRNA and EPX protein levels in nasal polyp tissues from patients with CRSwNP were detected by RT-qPCR and Western blotting. **(B)** Schematic diagram showing the establishment of the CRSwNP mouse model and AAV-shEPX intervention protocol. **(C)**Representative images of H&E staining (upper panels) and PAS staining (lower panels) of nasal mucosal tissues from different groups, with quantification of eosinophil infiltration and PAS-positive goblet cells. Scale bars: 800 μm and 50 μm. **(D)** Mouse *Epx* mRNA and EPX protein levels in nasal mucosal tissues were determined by RT-qPCR and Western blotting. **(E)** IL-4 and IL-5 levels in nasal mucosal tissues and serum IgE levels were measured by ELISA. *P□0.05, **P□0.01, ***P□0.001, ****P□0.0001

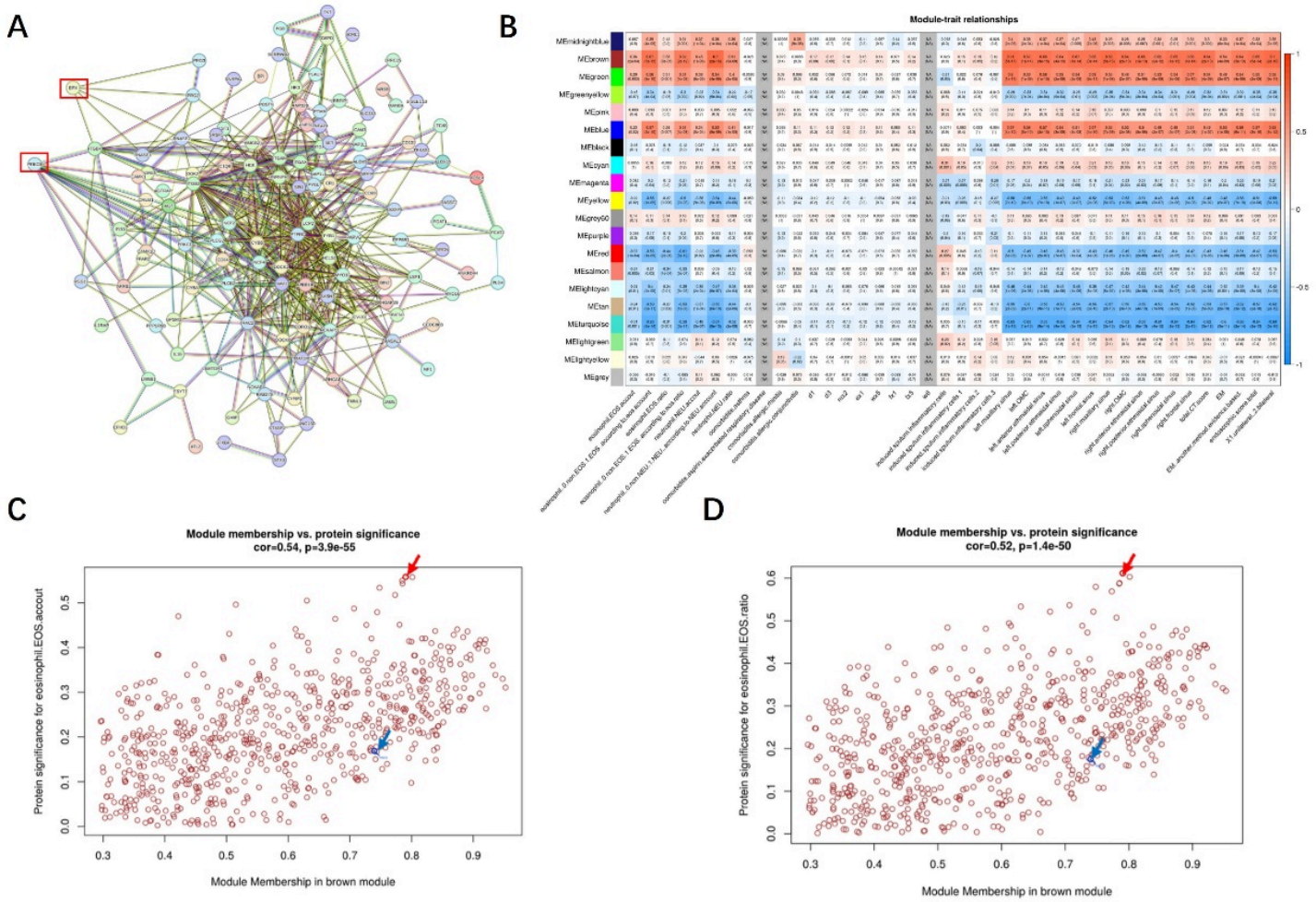


Figure 3

Association of EPX and PRKCB within the CRSwNP-associated protein co-expression network.(A) EPX-associated protein–protein interaction (PPI) network constructed from proteins significantly correlated with EPX expression (|r| > 0.6). EPX and PRKCB are highlighted by red and blue boxes, respectively. (B) WGCNA module–trait correlation heatmap showing associations of the brown module (MEbrown) with sinus CT scores, endoscopic scores, and peripheral blood inflammatory cell-related parameters. (C–D) Correlations between module membership (MM) and protein significance (PS) among proteins in the brown module. (C) PS analysis based on the absolute peripheral blood eosinophil count. (D) PS analysis based on the peripheral blood eosinophil proportion. EPX and PRKCB are indicated by red and blue arrows, respectively.

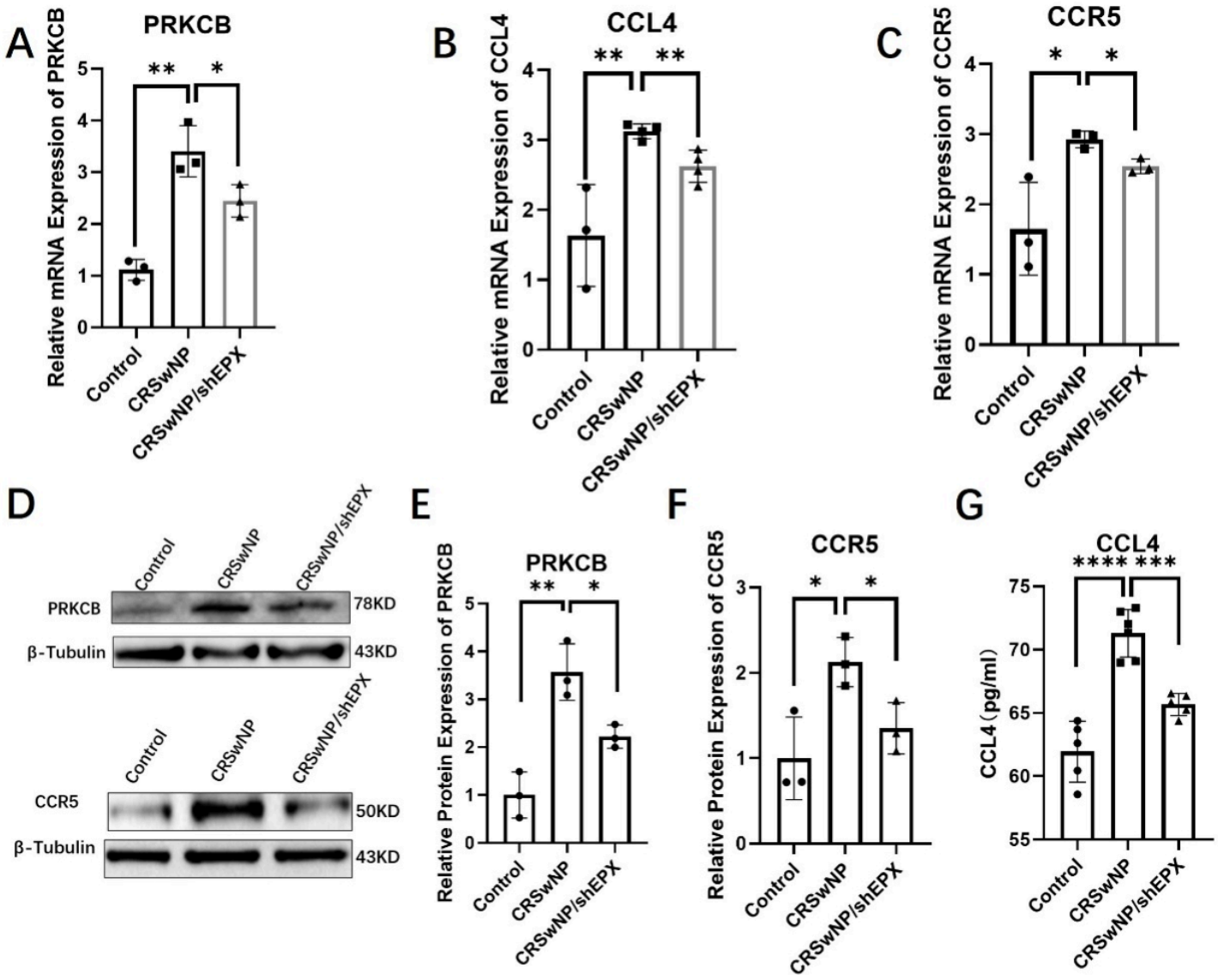


Figure 4

Effects of EPX knockdown on the expression of PRKCB/CCL4/CCR5-related molecules in the nasal mucosa of CRSwNP mice.(A–C) Mouse *Prkcb*, *Ccl4*, and *Ccr5* mRNA levels in nasal mucosal tissues from different groups detected by RT-qPCR. **(D–F)** PRKCB and CCR5 protein levels in nasal mucosal tissues assessed by Western blotting and densitometric analysis. **(G)** CCL4 protein levels in nasal mucosal tissues measured by ELISA. Data are presented as the mean ± SD. For RT-qPCR and Western blotting, n = 3 mice per group; for CCL4 measurement by ELISA, n = 5 mice per group. *P□0.05, **P□0.01, ****P□0.0001

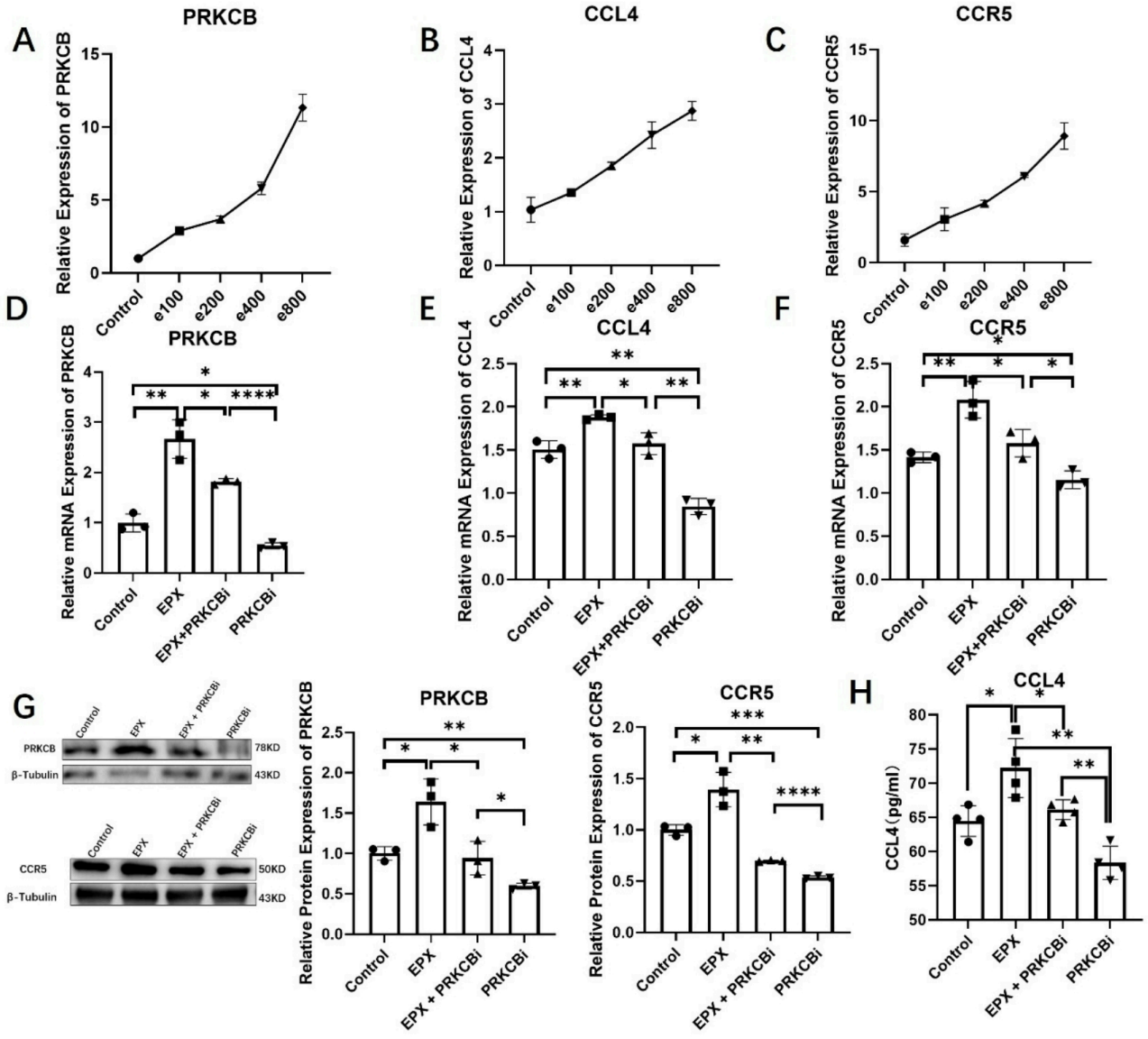


Figure 5

Effects of PRKCB inhibition on EPX-induced expression of CCL4/CCR5-related molecules in HNEpCs. **(A–C)** Human *PRKCB*, *CCL4*, and *CCR5* mRNA levels in HNEpCs stimulated with different concentrations of EPX, as determined by RT-qPCR. **(D–F)**Human *PRKCB*, *CCL4*, and *CCR5* mRNA levels in HNEpCs following EPX stimulation with or without PRKCB inhibitor treatment, as determined by RT-qPCR. **(G)**PRKCB and CCR5 protein levels in HNEpCs assessed by Western blotting and densitometric analysis. **(H)** CCL4 protein levels in cell culture supernatants measured by ELISA. Data are presented as the mean ± SD from three independent experiments for RT-qPCR and Western blotting and four independent experiments for ELISA. *P□0.05, **P□0.01, ***P□0.001, ****P□0.0001

Supplementary Files

This is a list of supplementary files associated with this preprint. Click to download.

- SupplementaryTableS1.docx